Hydrogen intercalation in MoS_{2}

Zhen Zhu, Hartwin Peelaers, and Chris G. Van de Walle

Phys. Rev. B **94**, 085426 — Published 25 August 2016

DOI: 10.1103/PhysRevB.94.085426

Hydrogen intercalation in MoS_2

Zhen Zhu,* Hartwin Peelaers, and Chris G. Van de Walle
Materials Department, University of California, Santa Barbara, CA 93106-5050, USA

We investigate structure and energetics of interstitial hydrogen and hydrogen molecules in layered 2H-MoS_2, an issue of interest both for hydrogen storage applications and for use of MoS_2 as an (opto)electronic material. Using first-principles density functional theory we find that hydrogen interstitials are deep donors. H_2 molecules are electrically inactive, and energetically more stable than hydrogen interstitials. Their equilibrium position is the hollow site of the MoS_2 layers. The migration barrier of a hydrogen molecule is calculated to be smaller than 0.6 eV. We have also explored the insertion energies of hydrogen molecules as a function of hydrogen concentration in MoS_2. For low concentrations, additional inserted H_2 molecules prefer to be located in hollow sites (on top of the center of a hexagon) in the vicinity of an occupied site. Once two molecules have been inserted, the energy cost for inserting additional H_2 molecules becomes much lower. Once all hollow sites are filled, the energy cost increases, but only by a modest amount. We find that up to 13 H_2 molecules can be accommodated within the same interlayer spacing of an areal 3×3 supercell.

PACS numbers: 61.72.-y, 66.30.J-, 73.22.-f, 88.30.R-.

I. INTRODUCTION

Among newly proposed energy resources, hydrogen, which is abundant and pollution free, is a highly promising candidate for use as a next-generation energy carrier. Significant advances have been made in recent years in hydrogen production[1] and storage.[2,3] However, finding higher-capacity hydrogen storage materials is still a priority. Layered MoS_2, which has long been known and used as a lubricant material,[4] is an attractive candidate for hydrogen storage[5] due to the weak interlayer interactions (van der Waals bonding) and the relatively large interlayer spacing.[6] Good performance for hydrogen storage has already been demonstrated with MoS_2 nanotubes;[7,8] in bulk MoS_2 high temperatures and pressures are required to obtain hydrogen intercalation.[9] To improve hydrogen-storage properties, a deeper understanding of the interaction between hydrogen and MoS_2 is essential.

2H-MoS_2, which is a semiconductor, has also drawn attention for (opto)electronic applications,[10] due to its large band gap[11–13] and favorable carrier mobility.[14] Since hydrogen is easily incorporated and electrically active in MoS_2 , knowledge about the electronic behavior of hydrogen impurities is important. Previous studies mainly focused on the behavior of hydrogen at the surface of MoS_2. Molecular hydrogen can dissociate near the surface of defective MoS_2 at elevated temperatures, rendering MoS_2 an effective catalyst for the hydrodesulfurization process.[15] Hydrogenation of the surface of MoS_2 has been realized, and formation of atomic stripes due to hydrogen-sulfur chemical bonds was observed.[16] Surface hydrogenation was also explored theoretically by investigating the interaction of atomic hydrogen with mono- and bilayer MoS_2 and it was predicted that hydrogenation transforms semiconducting to metallic MoS_2.[17,18] However, reliable information about hydrogen interactions with bulk MoS_2 is still lacking, in particular about the thermodynamics and kinetics of hydrogen insertion, mainly due to a lack of a proper approach to accurately describe the interlayer interactions and the electronic properties.[19–22]

The use of a hybrid functional in density functional theory (DFT) offers significant improvements in describing electronic structure, and when combined with the inclusion of van der Waals interactions provides accurate results for structural and electronic properties of layered materials such as MoS_2.[23,24] Here we study the interactions of hydrogen with MoS_2, using a hybrid functional with inclusion of van der Waals interactions to explore the equilibrium geometry, formation energy, and electronic behavior of interstitial H and H_2 molecules inside layered MoS_2 structures. We also investigate H_2 migration barriers and the energy required to insert additional H_2 molecules in MoS_2 as a function of the hydrogen concentration.

Section II outlines our computational methodology. In Sec. III, we first describe the structural and electronic properties of pristine MoS_2 (Sec. III A), followed by the properties of hydrogen interstitials and hydrogen molecules inside MoS_2 (Sec. III B). We then discuss the migration of hydrogen molecules (Sec. III C) and the energetics of multiple hydrogen molecules in MoS_2 (Sec. III D). Section IV concludes the paper.

II. COMPUTATIONAL METHODS

All our calculations are based on DFT using projector-augmented waves[25] (PAW) as implemented in the VASP[26,27] code. We use periodic boundary conditions and supercell structures to study the interaction of hydrogen (in both atomic and molecular forms) with layered MoS_2. Formation energy calculations are performed using the screened hybrid functional of Heyd, Scuseria and Ernzerhof (HSE).[28,29] We have used standard values for the mixing parameter (0.25) and the range-separation parameter (0.2 $Å^{-1}$), and a 350 eV energy cutoff. We have

explicitly included the van der Waals interactions based on the vdW-D2 method;[30,31] an evaluation of a number of different functionals[23] indicated that the combination of HSE with D2 yielded an optimal description of both electronic and structural properties of MoS_2. For the bulk MoS_2 calculations we used a $6\times6\times2$ k-point grid[32] and an equivalent k-point sampling in Perdew, Burke, and Ernzerhof (PBE)[33] calculations for supercell structures; a single k-point (0.25,0.25,0.25) is used for HSE calculations in the large supercell structures. Use of the hybrid functional would be computationally prohibitive for the large number of calculations required to study migration and insertion of hydrogen molecules; these aspects were studied with the PBE functional, also combined with the vdW-D2 method. Calculations for test structures indicated that for interstitial H_2 molecules the difference in calculated formation energies between PBE-D2 and HSE-D2 is small, less than 0.01 eV, and that the equilibrium structures are very similar. The structures are relaxed until all forces are smaller than 0.02 eV/Å. Spin polarization was included, which reduces the total energy in case an unpaired electron is present.

The stability of a hydrogen interstitial H_i in MoS_2 can be assessed by studying its formation energy,[34] defined as

$$E^f(\mathrm{H}_i^q) = E_{\rm tot}(\mathrm{H}_i^q) - E_{\rm tot}(\mathrm{MoS_2}) - \mu_{\rm H} + q\epsilon_F + \Delta^q, \quad (1)$$

and similarly for H_2 molecules:

$$E^f(\mathrm{H_2}) = E_{\rm tot}(\mathrm{H_2}) - E_{\rm tot}(\mathrm{MoS_2}) - 2\mu_{\rm H}. \quad (2)$$

Here $E_{\rm tot}(\mathrm{H}_i^q)$ is the total energy of an MoS_2 supercell containing the interstitial in charge state q, $E_{\rm tot}(\mathrm{H_2})$ the total energy of an MoS_2 supercell containing an H_2 molecule, and $E_{\rm tot}(\mathrm{MoS_2})$ the total energy of the pristine MoS_2 structure. μ_H is the chemical potential of hydrogen. For purposes of displaying our results, we set $\mu_{\rm H}$ equal to half of the total energy of an isolated H_2 molecule at $T=0$. However, results for other chemical-potential conditions can easily be obtained be referring back to Eqs. (1) and (2). ϵ_F is the Fermi energy, referenced to the valence-band maximum (VBM). Δ^q is a correction term that removes the spurious interaction of charged defects due to periodic boundary conditions.[35,36]

The charge-state transition level (q/q') of interstitial H can be calculated from the formation energies by

$$(q/q') = \frac{E^f(\mathrm{H}_i{}^q;\epsilon_F=0) - E^f(\mathrm{H}_i{}^{q'};\epsilon_F=0)}{(q'-q)}. \quad (3)$$

When the Fermi level is below this energy, the charge state q is stable; otherwise, the charge state q' is stable.

III. RESULTS AND DISCUSSIONS

A. Bulk MoS_2

The most stable phase of bulk MoS_2 is the semiconducting 2H phase. The primitive unit cell of 2H-MoS_2 contains two AB-stacked atomic layers and each layer forms a hexagonal lattice. The 2D layers are bound by weak van der Waals forces. We optimized the structure of 2H-MoS_2 using either PBE or HSE functionals, in both cases including the van der Waals interactions following the Grimme-D2 method.[30] These two functionals will be referred to as PBE-D2 and HSE-D2. The optimized lattice parameters are listed in Table I. Similar to previous studies,[23] HSE-D2 values are in excellent agreement with experiment, but PBE-D2 also yields lattice parameters that deviate from the experimental values by less than 1%. In addition, the interlayer binding energy obtained by HSE-D2 is 19.5 meV/Å^2, in close agreement with the value obtained by more advanced methods such as the random phase approximation (RPA)[37] (see Table I).

An important difference between PBE-D2 and HSE-D2 is that PBE-D2 underestimates the band gap of MoS_2 by $\sim$0.4 eV, while the HSE-D2 result is closer to the experimental value. The discrepancy between HSE-D2 and experimental measurement is partly due to excitonic effects which are not included in our calculations. In the following we report results for the HSE-D2 functional, unless otherwise noted.

B. Interstitial H and interstitial H_2 molecules

To model the incorporation of hydrogen in MoS_2 in the dilute limit, we have constructed a large $4\times4\times2$ supercell to avoid spurious interactions between the periodically repeated hydrogens and to prevent unrealistic structural relaxations. The lattice constants of the supercell are constrained to the bulk values, consistent with modeling the dilute limit. In Fig. 1, we show the optimized MoS_2 structures with interstitial H or hydrogen molecules in the most stable structural configurations.

For interstitial H, we find that its preferential position is near a S atom, where it forms a S-H bond. Interestingly, the position of the interstitial H with respect to the S atom depends on its charge state. In the neutral and negative charge states, the interstitial H is located at the antibonding site, shown in Fig. 1(a). The S-H

TABLE I. Calculated and observed structural and electronic properties of 2H-MoS_2. $a=|\vec{a_1}|=|\vec{a_2}|$ is the in-plane lattice constant and c is the lattice constant in the out-of-plane direction. E_g is the electronic band gap. E_b is the interlayer binding energy.

	PBE-D2	HSE-D2	RPA	Experiment
a (Å)	3.19	3.16	-	3.16[a]
c (Å)	12.40	12.33	-	12.31[a]
E_g (eV)	0.93	1.51	-	1.30[b]
E_b (meV/Å^2)	18.4	19.5	20.5[c]	-

[a] Ref. 38.
[b] Ref. 11.
[c] Ref. 37.

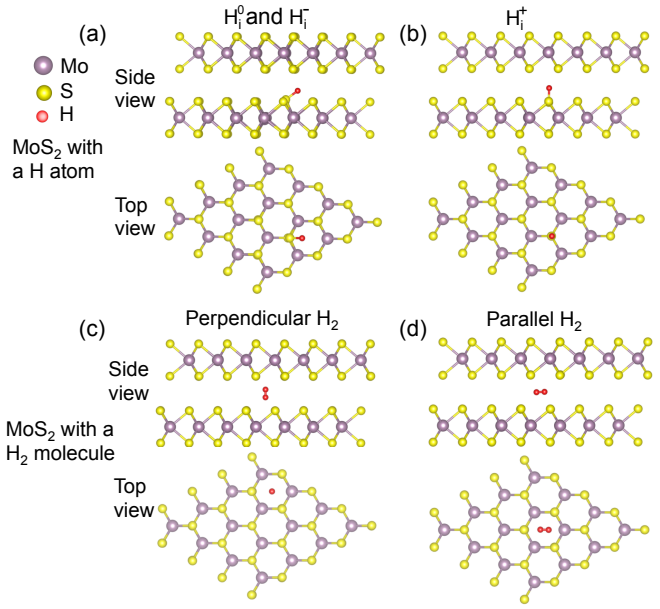

FIG. 1. (Color online) Atomic configurations of (a) H_i^0 (or H_i^-), (b) H_i^+, (c) perpendicular- and (d) parallel-aligned H_2 molecules in MoS_2 structures. Both side views and top views are provided.

bond is aligned with a Mo-S bond, pointing towards the interlayer spacing. The preferential position of the interstitial H in the positive charge state (H_i^+) is different: it favors a location on top of a S atom, with the S-H bond perpendicular to the MoS_2 layer.

Hydrogen molecules are electrically inactive and do not form covalent bonds with MoS_2. They are physisorbed in the interlayer space. We explored different positions and orientations of the H_2 molecule with respect to the MoS_2 layers, two of which are shown in Fig. 1. Figure 1(c) shows H_2 molecules aligned perpendicular to the MoS_2 layers, and Fig. 1(d) shows H_2 parallel to the layers. Both perpendicular H_2 and parallel H_2 are equidistant between two MoS_2 layers, and favor the hollow site of MoS_2, as this minimizes the expansion of the lattice in the interlayer direction and the repulsive interaction between H_2 with MoS_2. We find parallel H_2 to be the lowest-energy configuration with a formation energy of 0.80 eV. When parallel H_2 is rotated within the plane (around the hollow site it resides on), the different positions have very similar energies (differences < 10 meV). This will be relevant for the determination of migration barriers, as explained in detail in section III C.

In a $4 \times 4 \times 2$ supercell, the perpendicular H_2 structure is 0.19 eV less stable than parallel H_2, and is in fact not even a local minimum: a slight distortion off the perpendicular axis causes the molecule to relax to the parallel configuration. However, our investigation of the perpendicular configuration is useful in light of our studies of insertion of multiple H_2 molecules, as documented in Sec. III D. The higher energy of the perpendicular H_2 structure compared to the parallel H_2 configuration can be explained by the difference in the expansion of the interlayer spacing, which is larger for the perpendicular H_2, and thus costs more energy: insertion of a perpendicular H_2 inside MoS_2 expands the interlayer spacing by about 0.10 Å, while for parallel H_2, the expansion is smaller (0.07 Å). To make sure the effects of the interlayer expansion were accurately modeled we also carried out calculations in $3 \times 3 \times 3$ supercells. For perpendicular H_2, the energy in the $3 \times 3 \times 3$ supercell was 0.1 eV lower than in the $4 \times 4 \times 2$ supercell.

To gain insight into whether hydrogen in MoS_2 prefers the atomic or the molecular form, we can compare the formation energies of interstitial H in different charge states with the formation energy of an H_2 molecule (see Fig. 2). H_2 molecules are the lowest-energy configuration over the entire range of Fermi levels in the gap. Interstitial H in the positive charge state approaches the energy of H_2 in p-type material (Fermi level low in the gap), but MoS_2 tends to be n-type doped.[39] We conclude that hydrogen molecules are the preferred form of hydrogen in MoS_2.

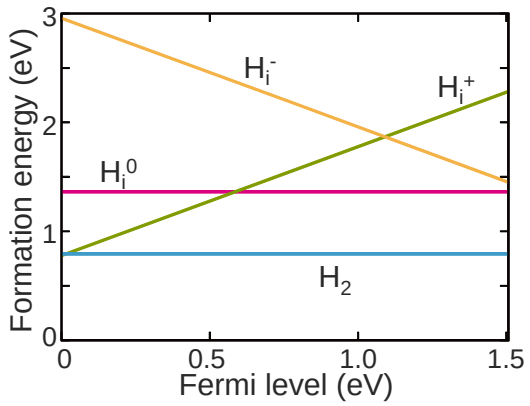

FIG. 2. (Color online) Formation energy as function of Fermi level for interstitial H and interstitial H_2 molecules in MoS_2. The zero of Fermi energy corresponds to the VBM, and the H chemical potential is set to half the energy of an H_2 molecule at $T = 0$.

Even so, information about interstitial H_i is important because in some cases hydrogen may be introduced into the layers in atomic form, and in order to assess how it may interact with other impurities or defects knowledge about its electronic behavior is essential. Figure 2 shows that the negative charge state is never stable, i.e., only the positive and neutral charge states can occur. The (+/0) transition level occurs at 0.58 eV above the VBM, indicating that H_i^+ is a deep donor, with the neutral charge state preferred over a large range of Fermi levels.

The point where the positive and negative charge states have equal formation energy, i.e., the (+/−) transition level, carries special significance in a semiconductor, since it probes the charge neutrality level and has been shown to exhibit a universal alignment across a wide

range of semiconductors and insulators.[40] For H_i in MoS_2 the (+/−) level occurs at 0.42 eV below the conduction-band minimum (CBM). In previous work[13] the position of the CBM referenced to the vacuum level was found to be at -4.25 eV , and therefore the (+/−) transition level is at -4.67 eV on an absolute energy scale; this value is consistent with the universal alignment of the hydrogen level at around -4.5 eV.[40]

C. Migration of H_2 molecules

As discussed in the previous section, H_2 molecules are the energetically favored form of hydrogen in MoS_2. To study their kinetics we calculated the migration barrier for an H_2 molecule moving between two equivalent neighboring equilibrium sites, using the climbing image nudged-elastic band method.[41,42] As noted in the Methods section, PBE-D2 suffices for calculations of the migration path.

We use 5 images to determine the migration pathway between neighboring equilibrium positions. The relaxed images are shown in Fig. 3(a) and the relative energies corresponding to these structures are shown in Fig. 3(b). Structure 1 is the initial state of the migration process, corresponding to the ground-state configuration of an H_2 molecule [Fig 1(d)]. The final structure [not depicted in Fig. 3(a)] is identical to structure 1, but with the H_2 molecule translated by a lattice vector. To migrate, the H_2 molecule first rotates 30°, so that it is oriented parallel to the edge of the Mo-S hexagon. This rotation requires less than 10 meV. The molecule then moves towards the edge of the hexagon. Image 4 of Fig. 3(a) corresponds to the saddle point of the migration pathway, with the H_2 molecule on top of the edge of the hexagonal ring, and one H atom located on top of a Mo atom. The energy of the saddle point yields a migration barrier of 0.53 eV.

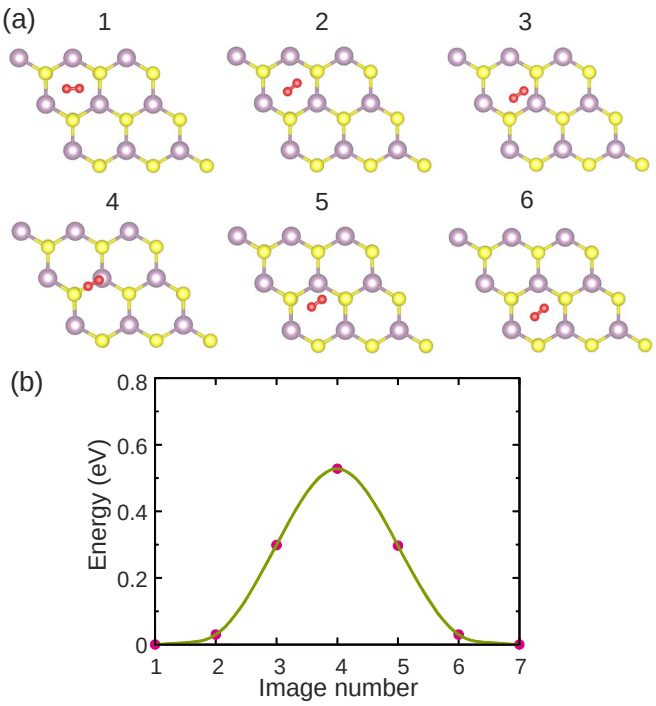

FIG. 3. (Color online) (a) Migration pathway and (b) potential energy for a parallel H_2 molecule migrating between two neighboring stable sites. Image 1 in (a) is the initial stable structure. Image 4 in (a) shows the structure corresponding to the saddle point.

D. Insertion of multiple H_2 molecules

Now that we have discussed the behavior of a single H_2 molecule in MoS_2, we consider what happens when additional H_2 molecules are inserted. For this study we employ a $3 \times 3 \times 1$ supercell, where we allow the lattice to relax upon insertion of multiple H_2 molecules. This mimics the situation where H_2 molecules are inserted in between every other layer of the crystal (one unit cell along the c direction contains two layers). To describe the energy cost required to insert the nth H_2 molecule, given that $(n-1)$ H_2 molecules have already been inserted, we define the insertion energy as

$$E_{\rm ins}^n = E_{\rm tot}[n{\rm H}_2] - E_{\rm tot}[(n-1){\rm H}_2] - 2\mu_{\rm H}. \qquad (4)$$

Here, $E_{\rm tot}[n{\rm H}_2]$ is the total energy of a MoS_2 supercell with n inserted H_2 molecules, and $\mu_{\rm H}$ is the chemical potential of hydrogen. For purposes of reporting our results, we set $\mu_{\rm H}$ equal to half of the energy of an isolated H_2 molecule at $T = 0$. We find that the insertion energy of the first H_2 in a relaxed $3\times3\times1$ supercell is 0.73 eV, consistent with the formation energy of a hydrogen molecule obtained in a constrained $4 \times 4 \times 2$ or $3 \times 3 \times 3$ supercell, as described in Sec. III B.

First, we explore the preferential position of a second H_2 molecule, when the first H_2 is situated in site A, as indicated in Fig. 4(a). We compare two different insertion sites, indicated in Fig. 4(a) and denoted by capital letters. A prime after the letter indicates that the position is located in the second layer within the cell. The calculated insertion energies for the second H_2 molecule $E_{\rm ins}^2$ at the different sites are shown in Fig. 4(b).

We find that it is energetically most favorable to add the second H_2 within the same interlayer spacing as the first H_2 molecule. The neighboring B site is only slightly more favorable then the next-nearest neighbor C site. The insertion energy is reduced from 0.73 eV for the first H_2 to 0.25-0.27 eV for a second molecule, because the interlayer spacing has already been expanded by the first H_2 molecule. Inserting a second H_2 molecule in the second interlayer spacing (primed sites) requires a similar amount of energy as for the first H_2 molecule [see Fig. 2 or the first data point of Fig. 4(b)], because it requires an expansion of the second interlayer spacing. Experimentally, an increased interlayer spacing can also be achieved

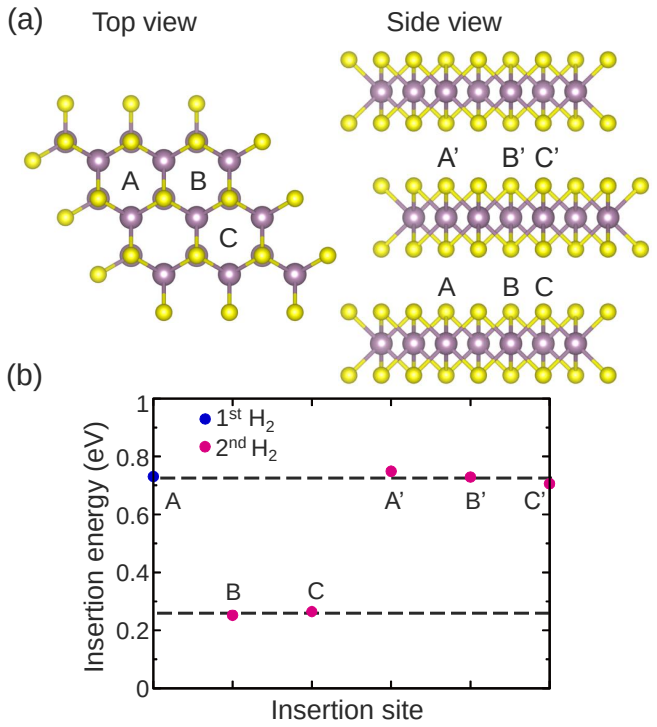

FIG. 4. (Color online) (a) Inequivalent insertion sites for a second H_2 molecule in a $3\times3\times1$ supercell when one molecule is already present at site A. (b) Dependence of the insertion energy for a second H_2 molecule on the insertion location, when one H_2 molecule is already present at site A. The dashed lines are guides to the eye.

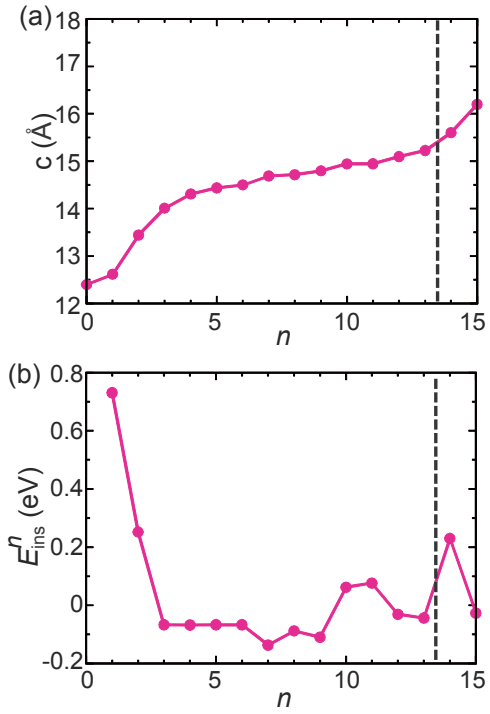

FIG. 5. (Color online) (a) Lattice constant c in the out-of-plane direction and (b) insertion energy of the n^{th} H_2 molecule as a function of n in a $3\times3\times1$ MoS_2 supercell. The dashed lines indicate the separation between $n = 13$ and $n = 14$, which is discussed in the main text. μ_H is set to half the energy of an H_2 molecule.

through a microwave-assisted technique,[43] which would reduce the hydrogen insertion energy, thereby facilitating the hydrogen incorporation process.

Since inserting H_2 molecules in the same interlayer spacing is energetically favored compared to a different interlayer spacing, we have focused on exploring the insertion process of multiple H_2 molecules within the same interlayer spacing. With increased H_2 density, the lattice constant along the out-of-plane direction increases [Fig. 5(a)], while the insertion energy of additional H_2 molecules decreases [Fig. 5(b)]. For $n > 2$, the additional energy required to insert an extra H_2 molecule becomes lower than the energy required to insert one or two H_2 molecules. The insertion energy is particularly low in the range $3\leq n\leq9$, where the values in Fig. 5(b) even become negative. We note, however, that these absolute values of insertion energies depend on the value of μ_H chosen in the definition of the insertion energy [Eq. (4)].

It turns out we can insert up to n=13 H_2 molecules within the same interlayer in the areal 3×3 supercell, with the c lattice constant staying at a plateau value [Fig. 5(a)]. At n=14, however, the c lattice constant increases, accompanied by a jump in the insertion energy [Fig. 5(b)].

This trend of insertion energy as a function of n can be explained by considering the optimized structures (Fig. 6). At low hydrogen concentrations, H_2 molecules are nearly parallel and aligned on hollow sites of MoS_2. With increasing n, H_2 molecules tilt to reduce the repulsion between nearby hydrogen molecules [Fig. 6(c)]. At $n = 9$, all hollow sites in the first layer are fully occupied. Additional H_2 molecules distort the already inserted H_2 molecules off the hollow sites, causing a rearrangement that minimizes the repulsion between the H_2 molecules. This rearrangement increases the insertion energy, but only by a modest amount (0.1-0.2 eV). For $n > 9$ the H_2 molecules are irregularly inserted in the MoS_2 interlayer spacing [Fig. 6(d)]. For these configurations, a lot of different orientations with similar energies are possible. Structurally, we find that the change of in-plane lattice constants is less than 1%, while the interlayer distance increases modestly with increasing H_2 concentration in the "plateau" region up to n=13 [Fig. 5(a)]. In this plateau region, the molecules are all arranged roughly with the same c coordinate. At n=14, however, the H_2 molecules rearrange in two layers (with different c coordinates) within the interlayer spacing of MoS_2. This requires a lattice expansion [Fig. 5(a)] and is also evident in the increase in insertion energy [Fig. 5(b)]. We conclude that n=13 molecules per 3×3 supercell is the maximum that can be accommodated without requiring an excessive change in the interlayer distance.

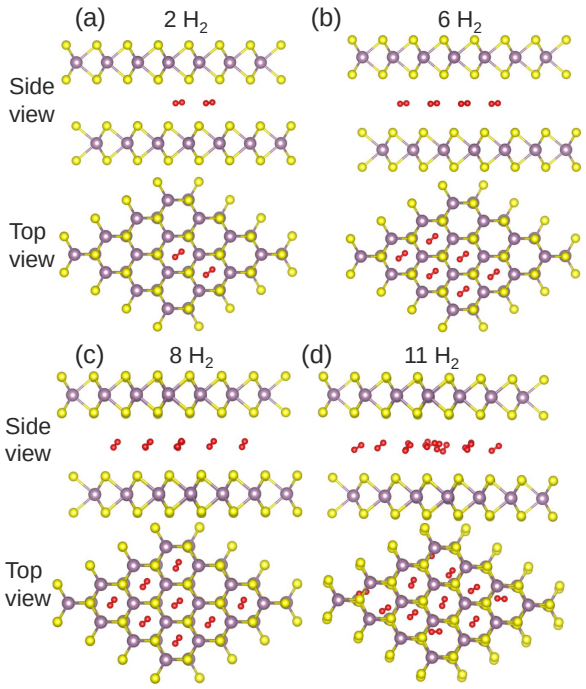

FIG. 6. (Color online) Equilibrium structures of MoS_2 in $3 \times 3 \times 1$ supercell with (a) two, (b) six, (c) eight, and (d) eleven H_2 molecules. Both side (top panel) and top (bottom panel) views are shown.

IV. CONCLUSIONS

In summary, we have investigated structure and energetics of interstitial hydrogen and H_2 molecules in MoS_2, in order to build a better understanding for hydrogen storage applications and for use of MoS_2 as an (opto)electronic material. Hydrogen interstitials act as deep donors, but their energy is higher than the energy of interstitial H_2 molecules. The equilibrium position of the molecules is in the hollow sites (above the centers of the hexagons) of the MoS_2 layers. The migration barrier of a hydrogen molecule is calculated to be 0.53 eV. We have also explored the insertion energies of hydrogen molecules as a function of hydrogen concentration in MoS_2. For low concentrations, additional inserted H_2 molecules prefer to be located in hollow sites in the vicinity of an occupied site. Once two H_2 molecules are present, the insertion of additional molecules can take place with much lower energy cost, up to the point that all hollow sites are occupied. Beyond this concentration, additional H_2 still prefer to go within the same interlayer spacing, with only a modest increase in insertion energy. Up to 13 H_2 molecules can be accommodated per 3×3 areal supercell without requiring a major change in the interlayer spacing.

V. ACKNOWLEDGEMENTS

This work was supported by the Office of Science of the U.S. Department of Energy (Grant No. DE-FG02-07ER46434). Computing resources were provided by the Center for Scientific Computing at the CNSI and MRL (an NSF MRSEC, Grant No. DMR-1121053) (Grant No. NSF CNS-0960316), and by the National Energy Research Scientific Computing Center, a DOE Office of Science User Facility supported by the Office of Science of the U.S. Department of Energy under Contract No. DE-AC02-05CH11231.

* zhuzhen@engineering.ucsb.edu

[1] Y. Jiao, Y. Zheng, M. Jaroniec, and S. Z. Qiao, Chem. Soc. Rev. **44**, 2060 (2015).
[2] D. J. Durbin and C. Malardier-Jugroot, Int. J. Hydrogen Energy **38**, 14595 (2013).
[3] P. Jena, J. Phys. Chem. Lett. **2**, 206 (2011).
[4] F. L. Claus, *Solid Lubricants and Self-Lubricating Solids* (Academic Press, New York, NY, 1972).
[5] S. B. Nikishenko, A. A. Slinkin, G. V. Antoshin, K. M. Minachev, and B. K. Nefedov, Kinet. Catal. **23**, 695 (1982).
[6] V. A. Makara, N. G. Babich, N. I. Zakharenko, V. A. Pasechny, O. V. Rudenko, V. F. Surzhko, L. M. Kulikov, A. A. Semenov-Kobzar, M. M. Antonova, A. A. Chekhovsky, L. G. Askel-Rud, and L. P. Romaka, Int. J. Hydrogen Energy **22**, 233 (1997).
[7] J. Chen, N. Kuriyama, H. Yuan, H. Takeshita, and T. Sakai, J. Am. Chem. Soc. **123**, 11813 (2001).
[8] J. Chen, S. Li, and Z. Tao, J. Alloys Compd. **356**, 413 (2003).
[9] Z. Paál, P. G. Menon, and M. Dekker, *Hydrogen Effects in Catalysis: Fundamentals and Practical Applications* (Taylor & Francis, New York, 1987).
[10] Q. H. Wang, K. Kalantar-Zadeh, A. Kis, J. N. Coleman, and M. S. Strano, Nature nanotechnology **7**, 699 (2012).
[11] A. R. Beal and H. P. Hughes, J. Phys. C Solid State Phys. **12**, 881 (1979).
[12] K. F. Mak, C. Lee, J. Hone, J. Shan, and T. F. Heinz, Phys. Rev. Lett. **105**, 136805 (2010).
[13] J. E. Padilha, H. Peelaers, A. Janotti, and C. G. Van de Walle, Phys. Rev. B **90**, 205420 (2014).
[14] B. Radisavljevic, A. Radenovic, J. Brivio, V. Giacometti, and A. Kis, Nature nanotechnology **6**, 147 (2011).
[15] A. Sierraalta, O. Lisboa, and L. Rodriguez, Journal of Molecular Structure: THEOCHEM **729**, 91 (2005).
[16] S. W. Han, W. S. Yun, J. D. Lee, Y. H. Hwang, J. Baik, H. J. Shin, W. G. Lee, Y. S. Park, and K. S. Kim, Phys. Rev. B **92**, 241303 (2015).
[17] I. Yakovkin and N. Petrova, Chemical Physics **434**, 20 (2014).
[18] Y. Cai, Z. Bai, H. Pan, Y. P. Feng, B. I. Yakobson, and Y.-W. Zhang, Nanoscale **6**, 1691 (2014).
[19] E. W. K. Koh, C. H. Chiu, Y. K. Lim, Y.-W. Zhang, and H. Pan, Int. J. Hydrogen Energy **37**, 14323 (2012).
[20] M. D. Ganji, N. Sharifi, M. G. Ahangari, and A. Khosravi, Physica E **57**, 28 (2014).

[21] D. B. Putungan, S.-H. Lin, C.-M. Wei, and J.-L. Kuo, Phys. Chem. Chem. Phys. **17**, 11367 (2015).

[22] Y. Yuan, X. Gong, and H. Wang, Phys. Chem. Chem. Phys. **17**, 11375 (2015).

[23] H. Peelaers and C. G. Van de Walle, J. Phys. Condens. Matter **26**, 305502 (2014).

[24] H. Peelaers and C. G. Van de Walle, J. Phys. Chem. C **118**, 12073 (2014).

[25] P. E. Blöchl, Phys. Rev. B **50**, 17953 (1994).

[26] G. Kresse and J. Furthmüller, Phys. Rev. B **54**, 11169 (1996).

[27] G. Kresse and J. Furthmüller, Comput. Mater. Sci. **6**, 15 (1996).

[28] J. Heyd, G. E. Scuseria, and M. Ernzerhof, J. Chem. Phys. **118**, 8207 (2003).

[29] J. Heyd, G. E. Scuseria, and M. Ernzerhof, J. Chem. Phys. **124**, 219906 (2006).

[30] S. Grimme, J. Comput. Chem. **27**, 1787 (2006).

[31] T. Bučko, J. Hafner, S. Lebègue, and J. G. Ángyán, J. Phys. Chem. A **114**, 11814 (2010).

[32] H. J. Monkhorst and J. D. Pack, Phys. Rev. B **13**, 5188 (1976).

[33] J. P. Perdew, K. Burke, and M. Ernzerhof, Phys. Rev. Lett. **77**, 3865 (1996).

[34] C. Freysoldt, B. Grabowski, T. Hickel, J. Neugebauer, G. Kresse, A. Janotti, and C. G. Van de Walle, Rev. Mod. Phys. **86**, 253 (2014).

[35] C. Freysoldt, J. Neugebauer, and C. G. Van de Walle, Phys. Rev. Lett. **102**, 016402 (2009).

[36] C. Freysoldt, J. Neugebauer, and C. G. Van de Walle, Phys. Status Solidi B **248**, 1067 (2011).

[37] T. Björkman, A. Gulans, A. V. Krasheninnikov, and R. M. Nieminen, Phys. Rev. Lett. **108**, 235502 (2012).

[38] R. Murray and B. Evans, J. Appl. Crystallogr. **12**, 312 (1979).

[39] Z. Wang, *MoS_2: Materials, Physics, and Devices*, Lecture Notes in Nanoscale Science and Technology (Springer International Publishing, 2013).

[40] C. G. Van de Walle and J. Neugebauer, Nature **423**, 626 (2003).

[41] G. Henkelman, B. P. Uberuaga, and H. Jónsson, J. Chem. Phys. **113**, 9901 (2000).

[42] G. Henkelman and H. Jónsson, J. Chem. Phys. **113**, 9978 (2000).

[43] M.-R. Gao, M. K. Y. Chan, and Y. Sun, Nat Commun **6**, 7493 (2015).